



ISSN: 0067-2904

Synthesis and Characterization of α -Fe₂O₃ Nanoparticles Prepared by PLD at Different Laser Energies

Ghaith H. Jihad

Department of Physics, College of Science, University of Baghdad, Iraq

Received: 30/4/2021

Accepted: 16/6/2021

Abstract

In this paper, ferric oxide nanoparticles (Fe₂O₃ NPs) were synthesized directly on a quartz substrate in vacuum by pulse laser deposition technique using Nd:YAG laser at different energies (171, 201,363 mJ/pulse). The slides were then heated to 700° C for 1 hour. The structural, optical, morphological, and electrical properties were studied. The optical properties indicated that the prepared thin films have an energy gap ranging from 2.28 to 2.04 eV. The XRD results showed no lattice impurities for other iron oxide phases, confirming that all particles were transformed into the α -Fe₂O₃ phase during the heating process. The AFM results indicated the dependence of nanoparticles size on the laser energy. As the laser energy increased, the average grain size increased from 72.6 nm to 79.02 nm. Hall effect measurement indicated that the film was an n-type semiconductor.

Keywords PLD (pulse laser deposition), Fe₂O₃ (ferric oxide hematite), Nd:YAG laser .

تخليق وتوصيف الجسيمات النانوية α -Fe₂O₃ المحضرة بواسطة نبضات الليزر ذات الطاقات المختلفة

غيث هادي جهاد

قسم الفيزياء، كلية العلوم، جامعة بغداد، بغداد، العراق

الخلاصة

في هذا البحث ، تم تحضير الجسيمات النانوية لأوكسيد الحديد (Fe₂O₃) بتقنية الترسيب بالليزر النبضي في ظروف الفراغ على عينة كوارتز باستخدام ليزر Nd: YAG عند طاقات مختلفة (171, 201,363 mJ/pulse)، ثم تم تسخين الشرائح إلى 700 درجة مئوية لمدة ساعة واحدة، بحيث تم دراسة الخواص التركيبية والبصرية والمورفولوجية والكهربائية ، وأشارت الخواص البصرية إلى أن الأغشية الرقيقة المحضرة لها فجوة طاقة تتراوح من 2.28 إلى 2.04 فولت ، وأظهرت نتائج XRD عدم وجود شوائب شبيكية لمرحلة أكسيد الحديد الأخرى. ، مما يؤكد أن جميع الجزيئات قد تحولت إلى طور α -Fe₂O₃ أثناء عملية التسخين ، وأظهرت نتائج AFM اعتماد حجم الجسيمات النانوية على طاقة الليزر ، ومع زيادة طاقة الليزر ، زاد متوسط حجم الحبوب من 72.6 نانومتر إلى 79.02 نانومتر. أشار قياس تأثير هول إلى أن الغشاء كان من النوع n من أشباه الموصلات.

1. Introduction

In the recent years, iron oxide semiconductor with Hematite phase has been the center of many researchers attention. Fe₂O₃ is an n-type semiconductor with many advantages, such as

*Email: ghaith.jihad1104@sc.uobaghdad.edu.iq

narrow band gap energy of approximately 2.2 eV, low cost, non-toxicity, availability, and thermal stability [1, 2]. It has a great importance in optoelectronics, energy conversion, and solar cell applications. On the other hand [3-8], Fe₂O₃ nanoparticles can be synthesized by utilizing many techniques, such as microwave-assisted synthesis [9], thermal decomposition [10], chemical method [11], hydrothermal method [12], co-precipitation method [13], laser pyrolysis [14], and pulsed laser ablation, both in vacuum [15] or in liquid environment [16]. Pulsed laser deposition (PLD) is one of the most effective physical methods to produce nanoparticles. It produces nanoparticles with high quality, low cost, single step, and no contamination [17, 18].

Many studies discussing the formation of iron oxide nanoparticles by pulsed laser ablation were published in the past decade [15, 19 -22]. In this work, for the first time, the effects of laser energy change on the structural, morphological, optical, and electrical properties of iron nanoparticles are studied.

2. Materials and methods

Iron oxide powder (product #: 3310DX, 99% purity, SkySpring Nanomaterials Inc, Houston TX, USA) was pressed by a 10 tons hydraulic compressor for 1 minute into a pellet shape with a diameter of 16mm , high of 3mm, and weight of 2g. The iron oxide thin films were deposited on a quartz substrate by PLD technique. Figure (1) demonstrates the PLD setup.

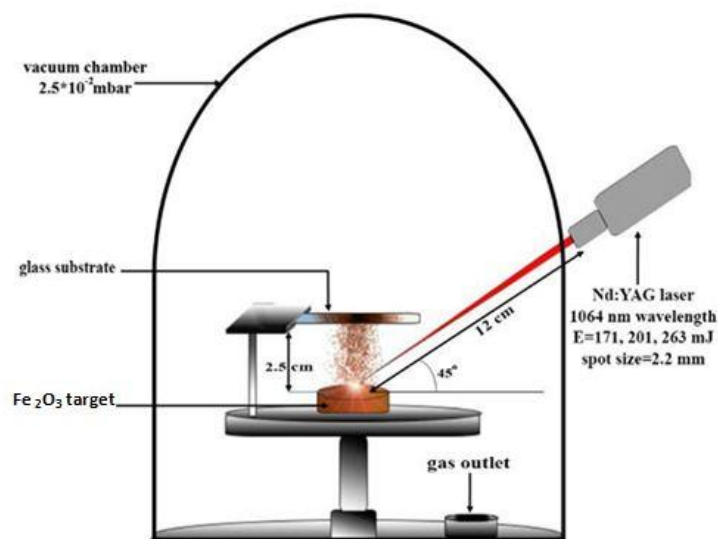


Figure 1-Schematic diagram of pulsed laser deposition under vacuum with Nd:YAG laser 1064nm .

The quartz slides were previously placed in an ultrasonic cleaner filled with DIW for 30 minutes. They were then placed in methanol for 10 minutes and finally air dried in order to eliminate all traces of contamination. The PLD chamber was evacuated to a pressure of 2.5×10^{-3} mbar using (Varian DS-219 rotary pump U.S.A) at room temperature (25°C). A Q-switched Nd:YAG laser (HF -301, Huafei technology, China) was used as a laser source. The number of pulses remained constant for all samples (200 pulses). The laser head was equipped with a focusing lens having a focal length of about 12 cm from the target. Table (1) lists the laser parameters.

Table 1-Q-switched Nd:YAG laser parameters.

Energy (mJ/pulse)	Wavelength (nm)	Pulse duration (nm)	Frequency (Hz)	Spot size (mm)
171, 201, 263	1064	10	1	2.2

After laser deposition, the thin films were placed in an electric furnace at 700°C for one hour to transform the iron oxide into α -Fe₂O₃ phase. After annealing, the morphological, optical, electrical, and structural properties of the thin films were studied using atomic force microscope (AFM) (CSPM- Scanning probe microscope), SP-8001 UV/Visible Spectrophotometer (Metertech, Taiwan), Hall effect measurement system (HMS-3000 ECOPIA, South Korea), and XRD (D₂ phaser, Bruker, Karlsruhe, Germany), respectively.

3. Results and discussion

After annealing the samples at 700°C for an hour, the first change noticed was the change in thin films color from black to bright red, indicating the formation of α -Fe₂O₃ phase. Figure (2) shows the difference in samples color.

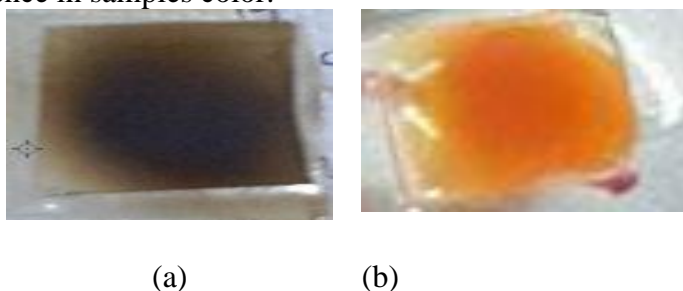


Figure 2-Iron oxide slides: (a) before annealing, (b) after annealing. Bright red color indicates hematite phase formation.

3.1. Structural properties

The XRD results for α -Fe₂O₃ NPs deposited on quartz at room temperature are shown in Figure (3-a). We notice that only two small peaks appear and the thin film behaves as amorphous structure due to short-ranged order. This result agrees with that reported by Al-Wardy [2]. In order to obtain the α -Fe₂O₃ diffraction peaks, the thin films were annealed at 700°C for an hour, as advised in Xavier [23], to completely transform the crystals to the hematite phase. The diffraction peaks were present at different energies, as shown in Figure (3-b).

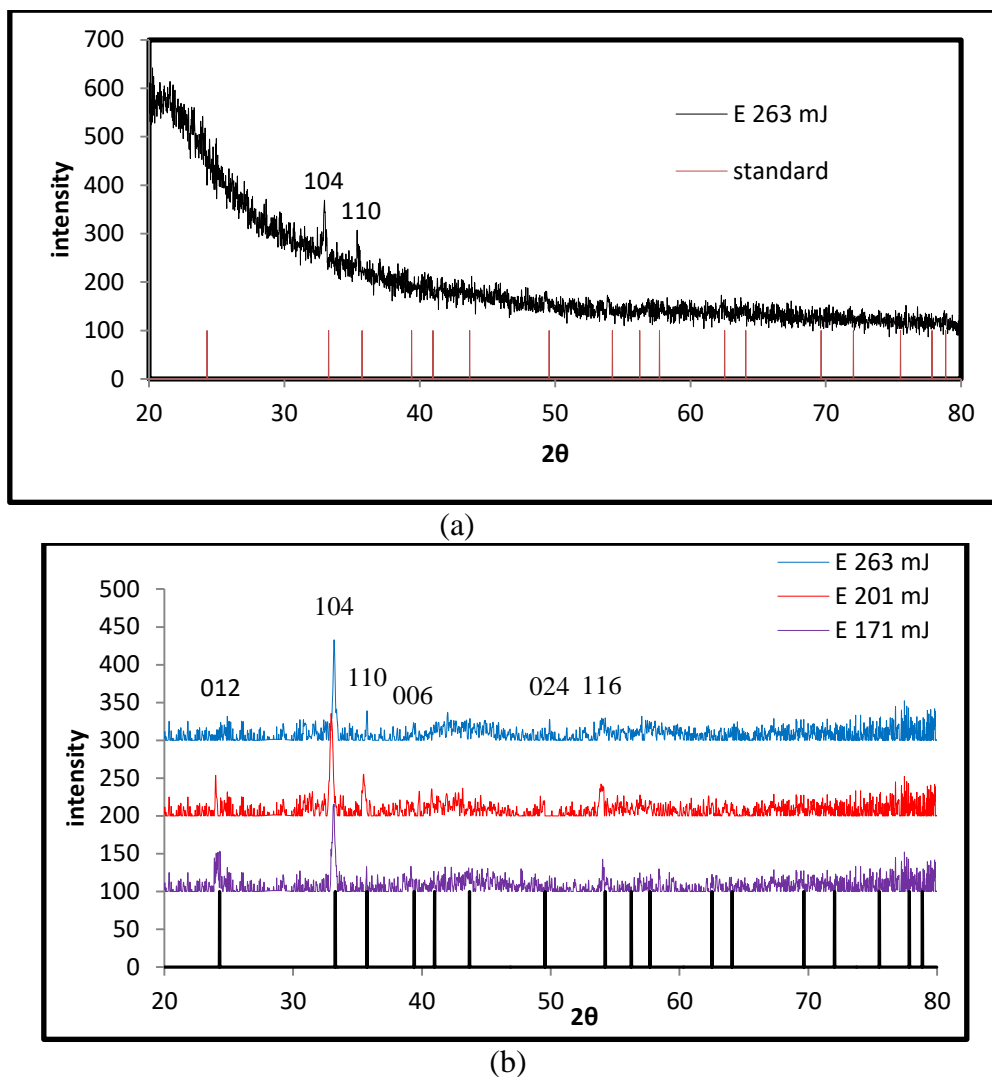


Figure 3-a- XRD pattern of α - Fe_2O_3 thin films at RT.(b) XRD pattern of α - Fe_2O_3 thin films at 700°C with different laser energies

The XRD patterns exhibit peaks centered at $2\theta = 24.2850^\circ$, 33.2743° , 35.7396° , 39.4017° , 49.5589° , and 54.2321° , corresponding to (012), (104), (110), (006), (024), and (116) planes, which are identical to the pure α - Fe_2O_3 card (JCPDS No. 86-0550), with close results to those obtained from previous studies [2, 23]. As the laser energy increases, the secondary peaks become present and the main peak increases slightly in width and height, as shown in Figure (3-b). Also, no other impurity peaks for other materials or iron phase are seen, indicating that the prepared thin films are of pure α - Fe_2O_3 . The standard d value (interplaner spacing) was calculated using Bragg formula [24] and compared with standard JCPDS card. The results are listed in table 2 along with the crystalline size values of the synthesized samples, which were calculated according to Scherrer's equation [25].

Table 2-the inter layer distance, crystalline size, and FWHM values of α -Fe₂O₃ NPs prepared at different energies.

E= 171 mJ/ Pulse					
2θ (deg.)	(hkl)	d_{hkl} Theo.(Å)	d_{hkl} Exp.(Å)	FWHM (deg.)	Crystalline size (nm)
24.2881	012	3.6600	3.6614	0.091	15.91
33.274	104	2.6901	2.6902	0.272	53.19
35.7398	110	2.5101	2.51012	0.059	24.69
39.4019	006	2.2010	2.2848	0.161	91.46
54.2325	116	1.6900	1.6898	0.083	18.76
E= 201 mJ/ Pulse					
2θ (deg.)	(hkl)	d_{hkl} Theo.(Å)	d_{hkl} Exp.(Å)	FWHM (deg.)	Crystalline size (nm)
24.2850	012	3.6600	3.66186	0.098	14.47
33.2743	104	2.6901	2.6902	0.274	52.81
35.7396	110	2.5101	2.5101	0.288	50.58
39.4017	006	2.2010	2.2848	0.122	12.07
49.5589	024	1.8380	1.83775	0.140	10.907
54.2321	116	1.6900	1.6899	0.377	41.31
E= 263 mJ/ Pulse					
2θ (deg.)	(hkl)	d_{hkl} Theo.(Å)	d_{hkl} Exp.(Å)	FWHM (deg.)	Crystalline size (nm)
33.2755	104	2.6901	2.69017	0.194	74.58
35.7392	110	2.5101	2.51017	0.105	13.873
39.4015	006	2.2010	2.28487	0.238	61.206
49.5584	024	1.8380	1.8377	0.076	20.09
54.2323	116	1.6900	1.6899	0.119	13.089

3.2. Surface morphology

AFM images of the samples are demonstrated in Figure 4-a, b and c for laser energies of 171 mJ, 201mJ, and 263 mJ, respectively. The average diameter, surface roughness, and RMS values are listed in Table (3).

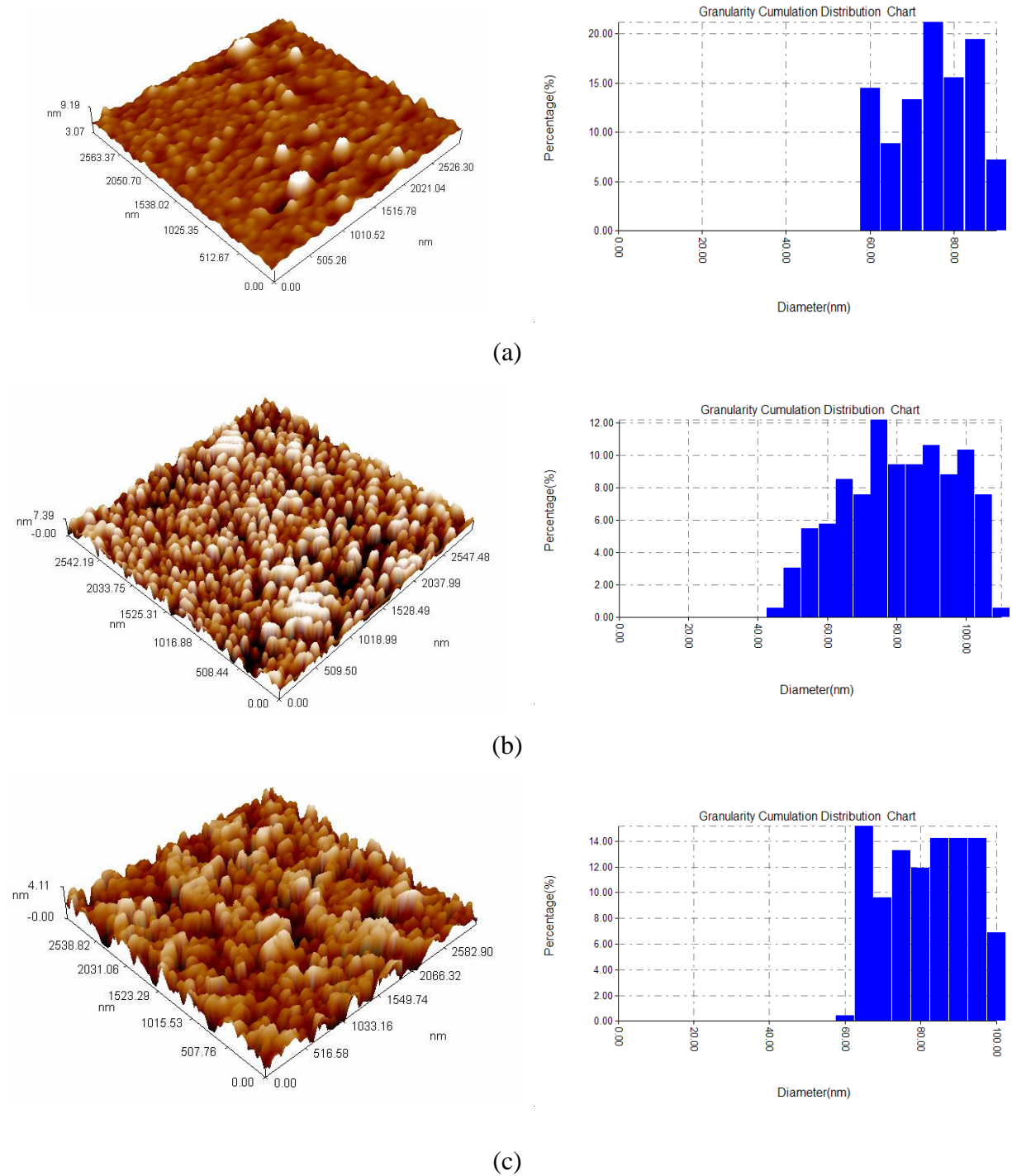


Figure 4- AFM surface images and average particles size of α -Fe₂O₃ NP samples prepared at (a) 171 mJ/pulse, (b) 201 mJ/pulse, and (c) 263 mJ/pulse.

Table 3-Average diameter, roughness, and RMS values of the synthesized of α -Fe₂O₃ NP films at different energies.

Laser energy (mJ/Pulse)	Average grain size (nm)	Roughness (nm)	(RMS) (nm)
171	72.60	0.42	0.632
201	77.28	0.65	0.813
263	79.02	0.747	0.905

Based on the results, it appears that the laser energy has a direct impact on the average particle size. As the laser energy increases, the nanoparticle size increases as well. This result is similar to that reported by Agasti's study [26]. As the laser energy increases, it provides higher thermal and kinetic energy to the nanoparticles. This high energy increases the speed in which the ablated nanoparticles are hitting the quartz substrate, causing nanoparticles to obtain high surface mobility at the surface [27]. In order to reduce the high surface energy of the system, large clusters are formed. Hence, aggregations occur with an overall increase the nanoparticles grain size [28].

3.3. Optical properties

Figure (5) demonstrates the relation between wavelength and absorption at different laser energies. The higher the laser energy, the larger is the size of nanoparticles ablated from the target surface. This causes the thin film thickness to increase, hence increasing absorption. A similar behavior was previously reported with ZnS thin films by Hamed [29].

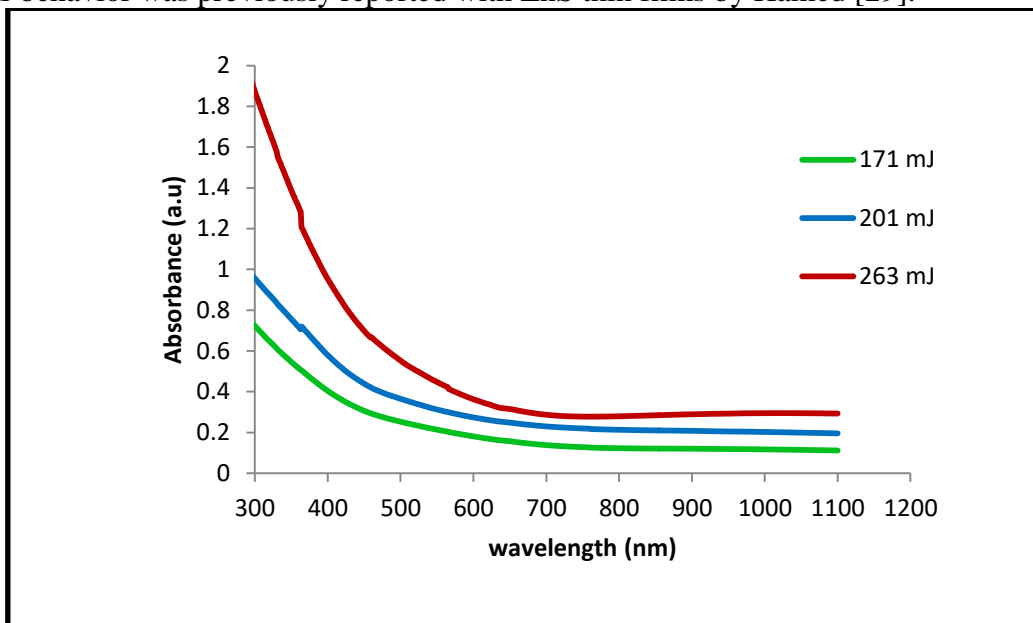


Figure 5-Absorption spectrum of α -Fe₂O₃ thin films prepared by PLD at different energies at 200 pulses.

The Fizeu fringes method was used to calculate the films thickness, employing the equation:

$$t = \frac{\lambda \Delta X}{2 X}$$

where ΔX is the distance between two successive fringes and X is the width of the fringe. In the PLD technique, the ablation rate is directly proportional to the laser energy, i.e. as the laser energy increases, a higher film thickness is obtained. The results are listed in Table 4.

Then, the optical band gap was graphically found using Tauc's formula [30] for direct transition:

$$(\alpha h\nu)^2 = A^2 (h\nu - E_g) \tag{1}$$

where E_g is the optical energy gap, α is the absorption coefficient, $h\nu$ is the photon energy of incident light, and A is a constant. The thickness of thin films was measured using optical an interferomete, as shown in Table (4).

Table 4 -shows the measurement of thickness of thin film at different energies.

Energy (mJ/pulse)	171	201	263
Thickness (nm)	135.1	140.2	186.8

The graph presented in Figure (6) reveals that as the laser energy increases, the optical band gap decreases. This can be attributed to the shift of absorption edge to higher wavelengths due to the increase in particle size, as demonstrated in the AFM results [31]. Table 5 illustrates the band gap energies at different laser fluencies.

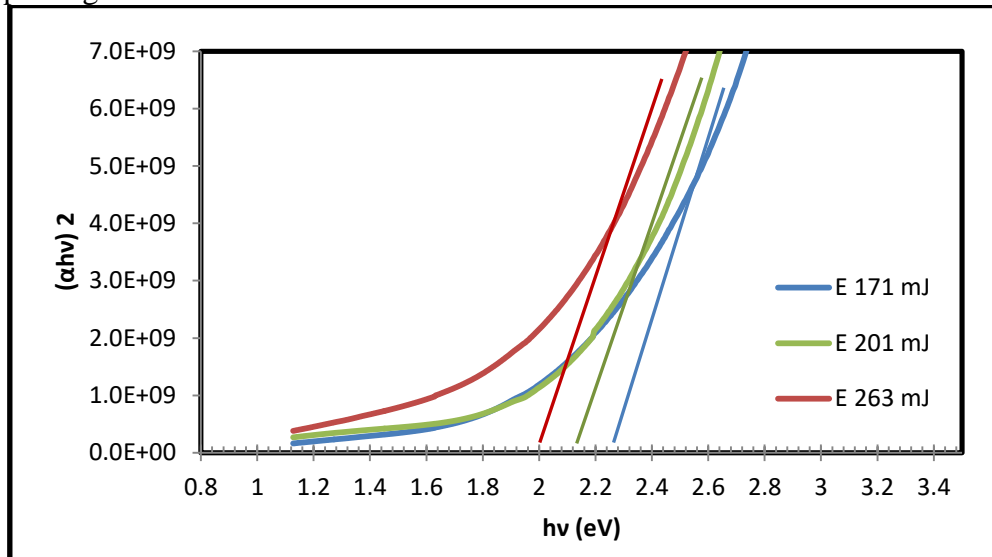


Figure 6-The $(\alpha hv)^2$ versus $h\nu$ plot for $\alpha\text{-Fe}_2\text{O}_3$ NPs prepared at different laser energies.

Table 5-Direct band gap energies at different laser fluencies

Laser energy (mJ/Pulse)	Energy gap (e.v)
171	2.28
201	2.16
263	2.04

3.4. Hall Effect

The conductivity type of the prepared thin films was identified by Hall effect measurement. Table (6) includes the Hall effect parameters of $\alpha\text{-Fe}_2\text{O}_3$ NPs prepared at 200 pulse and laser energies of 171 and 263 mJ. Hall effect measurements indicated that the obtained thin film is an n-type semiconductor, a result that agrees with previous reports [2, 3]. Due to the decrease of gap energy shown in optical properties, the number of charge carriers (n_0) was increased as the laser energy increased. Increasing the number of charge carriers leads to an increase in the conductivity (σ), along with decreasing the mobility (μ) and resistivity (ρ). Therefore, the value of Hall coefficient (R_H) is reduced.

Table 6-Results of Hall effect parameters of $\alpha\text{-Fe}_2\text{O}_3$ at different laser energies.

E (mJ/Pulse)	R_H (m^2/C)	σ ($\Omega.\text{cm}$) ⁻¹	ρ ($\Omega.\text{cm}$)	n_0 (cm^{-3})	μ ($\text{cm}^2/\text{V.s}$)
171	-4.181×10^5	2.202×10^{-5}	4.542×10^4	-1.615×10^{12}	9.207×10^0
201	-4.002×10^5	2.252×10^{-5}	4.412×10^4	-1.541×10^{12}	9.101×10^0
263	-3.902×10^5	2.325×10^{-5}	4.302×10^4	-1.600×10^{13}	9.070×10^0

4. Conclusions

$\alpha\text{-Fe}_2\text{O}_3$ NPs were successfully synthesized by PLD technique at different energies. The results indicated that as the laser energy increases, particle size increases, causing a red shift

in the absorption spectrum and, therefore, decreasing the optical energy gap. As the energy gap decreases, the number of charged carriers increases, increasing conductivity and reducing mobility, resistivity, and Hall voltage. XRD results confirmed the purity of the α -Fe₂O₃ phase.

References

- [1] M. F. Al-Kuhaili, M. Saleem, and S. M. A. Durrani, "Optical properties of iron oxide (α -Fe₂O₃) thin films deposited by the reactive evaporation of iron," *J. Alloys Compd.*, vol. 521, pp. 178–182, 2012.
- [2] R. A. Al-wardy, H. A. T. Al-ogaili, and S. I. Abbas, "Study of Annealing Temperature on Prepared Iron oxide Nanoparticles by Sol-Gel Method," *Int. J. Innov. Res. Sci. Eng. Technol.*, vol. 5, no. 4, pp. 5560–5567, 2016.
- [3] N. V. Long, T. Teranishi, Y. Yang, C. M. Thi, Y. Cao, and M. Nogami, "Iron Oxide Nanoparticles for Next Generation Gas Sensors," *Int. J. Metall. Eng.*, vol. 1, no. December 2015, pp. 1–18, 2015.
- [4] S. S. Shinde, R. A. Bansode, C. H. Bhosale, and K. Y. Rajpure, "Physical properties of hematite α -Fe₂O₃ thin films: Application to photoelectrochemical solar cells," *J. Semicond.*, vol. 32, no. 1, pp. 1–8, 2011.
- [5] C. Wang, L. Wang, and K. Tang, "Synthesis of Mesoporous Fe₂O₃ Nanorods and Their Electrochemical Performance," *Int. J. Electrochemical Sci.*, vol. 8, pp. 4543–4550, 2013.
- [6] K. X. Wang, Z. Yu, V. Liu, M. L. Brongersma, T. F. Jaramillo, and S. Fan, "Nearly Total Solar Absorption in Ultrathin Nanostructured Iron Oxide for Efficient Photoelectrochemical Water Splitting," *ACS Photonics*, vol. 1, no. 3, 2014.
- [7] G. K. Dalapati, S. Masudy-Panah, A. Kumar, C. C. Tan, H. R. Tan, and D. Chi, "Aluminium alloyed iron-silicide/silicon solar cells: A simple approach for low cost environmental-friendly photovoltaic technology," *Sci. Rep.*, vol. 5, no. December, pp. 1–9, 2015.
- [8] S. Daothong, "Characterization of Fe₂O₃ Nanowires and its Solar Cell Applications," *Key Eng. Mater.*, vol. 766, pp. 217–222, 2018.
- [9] T. A. Lastovina, A. P. Budnyk, M. A. Soldatov, Y.V. Rusalev, A. A. Guda, A. S. Bogdan and A. V. Soldatov, "Microwave-assisted synthesis of magnetic iron oxide nanoparticles in oleylamine–oleic acid solutions," *Mendeleev Commun.*, vol. 27, no. 5, pp. 487–489, 2017.
- [10] A. Lassenberger, A. Lassenberger, T. A. Grünwald, P. D. J. van Oostrum, H. Rennhofer, H. Amenitsch, R. Zirbs, H. C. Lichtenegger and E. Reimhult, "Monodisperse Iron Oxide Nanoparticles by Thermal Decomposition: Elucidating Particle Formation by Second-Resolved in Situ Small-Angle X-ray Scattering," *Chem. Mater.*, vol. 29, no. 10, pp. 4511–4522, 2017.
- [11] J. B. Mamani, L. F. Gamarra, and G. E. de S. Brito, "Synthesis and characterization of Fe₃O₄ nanoparticles with perspectives in biomedical applications," *Mater. Res.*, vol. 17, no. 3, pp. 542–549, 2014.
- [12] H. Hayashi and Y. Hakuta, "Hydrothermal Synthesis of metal oxide nanoparticles in supercritical water," *Materials (Basel)*, vol. 3, no. 7, pp. 3794–3817, 2010.
- [13] P. L. Hariyani, M. Faizal, R. Ridwan, M. Marsi, and D. Setiabudidaya, "Synthesis and Properties of Fe₃O₄ Nanoparticles by Co-precipitation Method to Removal Procion Dye," *Int. J. Environ. Sci. Dev.*, vol. 4, no. 3, pp. 336–340, 2013.
- [14] R. Alexandrescu, V. Bello, V. Bouzas, R. Costo, and F. Dumitrache, "Iron Oxide Materials Produced by Laser Pyrolysis," pp. 22–25, 2010.
- [15] Mohammed M. Hameed, Abdul-Majeed E. Al-Samarai and Kadhim A. Aadim, "Synthesis and Characterization of Gallium Oxide Nanoparticles using Pulsed Laser Deposition" *Iraqi Journal of Science*, 2020, Vol. 61, No. 10, pp: 2582-2589
- [16] K. S. Khashan, G. M. Sulaiman, and R. Mahdi, "Preparation of iron oxide nanoparticles-decorated carbon nanotube using laser ablation in liquid and their antimicrobial activity," *Artif. Cells, Nanomedicine, Biotechnol.*, vol. 45, no. February, pp. 1–11, 2017.
- [17] Dalya K. Naser, Ahmed K. Abbas and Kadhim A. Aadim, "Zeta Potential of Ag, Cu, ZnO, CdO and Sn Nanoparticles Prepared by Pulse Laser Ablation in Liquid Environment," *Iraqi Journal of Science*, 2020, Vol. 61, No. 10, pp: 2570-2581.
- [18] K A Aadim, A Z Mohammad and M A Abduljabbar "Influence of laser energy on synthesizes

- of CdO/Nps in liquid environment,” IOP Conf. Series: Materials Science and Engineering 454 (2018) 012028 doi:10.1088/1757-899X/454/1/012028
- [19] C. Sima, C. Viespe, C. Grigoriu, G. Prodan, and V. Ciupina, “Production of oxide nanoparticles by pulsed laser ablation,” vol. 10, no. 10, pp. 2631–2636, 2008.
- [20] S. A. Mulencko, N. T. Gorbachuk, and N. Stefan, “Laser Synthesis of Nanometric Iron Oxide Films with High Seebeck Coefficient and High Thermoelectric Figure of Merit,” *Lasers Manuf. Mater. Process.*, vol. 1, no. 1–4, pp. 21–35, 2014.
- [21] I. P. Novoselova, A. P. Safronov, O. M. Samatov, A. I. Medvedev, and G. V. Kurlyandskaya, “Biocompatible Ferrofluids with Iron Oxide Nanoparticles Fabricated by Laser Target Evaporation,” *IEEE Magn. Lett.*, vol. 6, no. October, 2015.
- [22] I. P. Novoselova, O. M. Samatov, G. S. Kupriyanova, A. M. Murzakaev, A. P. Safronov, and G. V. Kurlyandskaya, “Magnetic Properties of Iron Oxide Nanoparticles Obtained by Laser Evaporation,” *Russ. Phys. J.*, vol. 59, no. 9, pp. 1491–1497, 2017.
- [23] A. M. Xavier, F. F. Ferreira, and F. L. Souza, “Morphological and structural evolution from akaganeite to hematite of nanorods monitored by ex situ synchrotron X-ray powder diffraction,” *RSC Adv.*, vol. 4, no. 34, pp. 17753–17759, 2014.
- [24] Y. Al-Douri, M. A. Fakhri, N. Badi, and C. H. Voon, “Effect of stirring time on the structural parameters of nanophotonic LiNbO₃ deposited by spin-coating technique,” *Optik (Stuttg.)*, vol. 156, pp. 886–890, 2018.
- [25] M. Zaien, K. Omar, and Z. Hassan, “Synthesis of dendrite - like petals of CdO nanostructure,” *Optoelectron. Adv. Mater. Rapid Commun.*, vol. 5, no. 9, pp. 982–984, 2011.
- [26] S. Beke, S. Giorgio, L. Korosi, L. Nanai, and W. Marine, “Structural and optical properties of pulsed laser deposited V₂O₅ thin films,” *Thin Solid Films*, vol. 516, no. 15, pp. 4659–4664, 2008.
- [27] R. Myerlas, “Key Parameters of Pulsed Laser Deposition for Solid Electrolyte Thin Film Growth,” 2017.
- [28] A. Happy, S.R. Mohanty, P. Lee, T.L. Tan, S.V. Springham, A. Patran, R.V. Ramanujan, R.S. Rawat, “Effect of deposition parameters on morphology and size of FeCo nanoparticles synthesized by pulsed laser ablation deposition,” *Appl. Surf. Sci.*, vol. 252, no. 8, pp. 2806–2816, 2006.
- [29] E. Hamed, “Laser energy effect on the properties of ZnS thin films prepared by PLD technique,” *Iraqi J. Phys.*, vol. 11, no. 21, pp. 84–90, 2013.
- [30] M. A. Fakhri, Y. Al-Douri, U. Hashim, and E. T. Salim, “Optical investigations of photonics lithium niobate,” *Sol. Energy*, vol. 120, pp. 381–388, 2015.
- [31] L. Filippini and D. Sutherland, *Nanotechnologies: Principles, Applications, Implications and Hands-on Activities*. Luxembourg: Publications Office of the European Union, 2012.